JMEPEG (2022) 31:742–752
https://doi.org/10.1007/s11665-021-06184-3

1059-9495/$19.00

Effect of Initial Microstructure Conditions on the Microstructure and Mechanical Properties of Hot Extruded Mg-6Nd-2Al Alloy

Chunqi Yu, Yicheng Feng, Jiapeng Zhang, Lei Wang, Sicong Zhao, and Liping Wang

Submitted: 17 June 2021 / Revised: 4 August 2021 / Accepted: 15 August 2021 / Published online: 7 September 2021

In the present paper, the effect of initial microstructure on the hot extruded Mg-6Nd-2Al alloy was carried out by microstructural observation and mechanical property testing. The results show that there are short rod-shaped $Al_{11}Nd_3$ phase, strip-shaped $Mg_{12}Nd$ phase and granular Al_2Nd phase in the as-cast Mg-6Nd-2Al alloy after hot extrusion. The as-cast alloy is treated by solid solution and then hot extrusion, the granular Al_2Nd phase can still be observed in the alloy, and the needle-shaped Al_2Nd phase precipitates inside the α-Mg matrix. A typical (0001) texture and {01-10} prismatic surface texture appear in the as-cast alloy after hot extrusion, while in the solid-solution alloy after hot extrusion does not form an obvious preferred orientation. The ultimate tensile strength and the yield strength of the as-cast alloy after hot extrusion are higher, which are 271.2MPa and 247.8MPa, respectively. However, the elongation of the as-cast alloy after hot extrusion is lower, which is 15.3%.

Keywords hot extrusion, Mg alloy, microstructure, mechanical properties, texture

1. Introduction

Magnesium alloys are used in automotive, aviation, aerospace and other industrial fields for their low density, low cost, good shock absorption, thermal conductivity and dimensional stability. They are also used in computers, communications, consumer electronics, medical equipment and other industries and are known as the green engineering material of the 21st century (Ref 1, 2). However, the strength and high temperature performance of magnesium alloys are poor, which limit the development and application of magnesium alloys (Ref 3, 4). Slippage is a major way of plastic deformation in magnesium alloys. Magnesium has a low number of active slip systems due to its hexagonal close-packed (HCP) crystal structure, resulting in difficulty in plastic deformation (Ref 5). Therefore, improving the strength and deformability of magnesium alloys are one of the current research hotspots.

Mg-RE alloys have excellent comprehensive properties, however, the as-cast Mg-RE alloy has coarse grain size and poor mechanical properties, which is usually refined in casting conditions (Ref 6). In recent years, researchers use Al instead of Zr to be added to the Mg-RE alloys, Al can refine the grains, and the cost is lower (Ref 7-10). RE will preferentially interact with Al to form an Al-RE phase with high temperature stability. The main second phases in Mg-RE-Al alloy are granular Al_2RE phase and needle-like $Al_{11}RE_3$ phase. Al_2RE phase is an effective nucleation point for the magnesium matrix and can improve the thermal stability of the refined Mg-RE alloys. In addition, Al_2RE and $Al_{11}RE_3$ phases can effectively hinder the movement of grain boundary slip and dislocations, so it can significantly improve the strength of the alloy (Ref 11, 12). In the Mg-RE-Al alloy after hot extrusion, the grains are significantly refined, and the mechanical properties are also significantly improved (Ref 13, 14). Pourbahari et al. studied Mg-Gd-Al-Zn alloys in as-cast, homogenized and extruded conditions. The results showed that the grains were refined in the extrusion process, and the tensile strength and elongation were improved compared with the original as-cast alloy (Ref 15). The initial texture on the extrusion AZ31 magnesium alloy significantly affected twinning behavior (Ref 16). Our research group found that the type, distribution, morphology and content of the second phase in the magnesium alloy affected the microstructure and mechanical properties of the Mg-6Al-2Ca-2Sm alloy after hot extrusion (Ref 17). Therefore, in the present paper, a Mg-6Nd-2Al alloy was designed, which contained needle-shaped $Al_{11}Nd_3$ phase and granular Al_2Nd phase. The Mg-6Nd-2Al alloy was isothermal treated, and the needle-shaped Al_2Nd phase was precipitation from the magnesium matrix. The as-cast and isothermal treated Mg-6Nd-2Al alloys were hot extruded, respectively. The microstructure and mechanical properties were observed and analyzed completely.

2. Materials and Methods

2.1 Material

To prepare Mg-6Nd-2Al alloy, Mg-30%Nd master alloy (wt.%), pure magnesium (Mg > 99.95 wt.%), pure aluminum (Al > 99.90 wt.%), and RJ-2 type covering agent were used.

Chunqi Yu, Yicheng Feng, Lei Wang, Sicong Zhao, and **Liping Wang**, School of Materials Science and Chemical Engineering, Harbin University of Science and Technology, Harbin 150040, China; **Jiapeng Zhang**, School of Materials Science and Chemical Engineering, Harbin University of Science and Technology, Harbin 150040, China; and AECC Harbin Dongan Engine Co, Ltd 150060 Harbin, China. Contact e-mail: wangxiaolei2005@126.com.

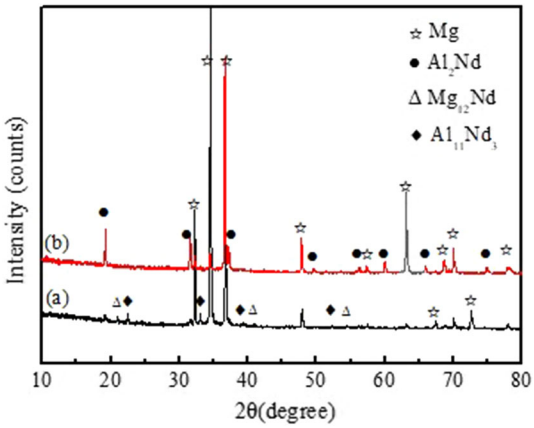

Fig. 1 XRD patterns of Mg-6Nd-2Al alloy for (a) the as-cast alloy after hot extrusion; (b) the solid-solution alloy after hot extrusion

First of all, the charge and metal mold were preheated at 300 °C. After that, all alloys were smelting in the pit resistance furnace at 720 °C, and were cast into a round ingot in a metal mold with the size of Φ60 mm × 120 mm to prepare as-cast Mg-6Nd-2Al alloy. In order to study the effect of initial microstructure conditions on the microstructure and mechanical properties of the hot extruded Mg-6Nd-2Al alloy, an as-cast Mg-6Nd-2Al alloy was isothermal treated in the SX2-4-10 box-type resistance furnace at 535 °C for 14 h. The as-cast and isothermal treated alloys were cut into ingots of Φ58 mm × 70 mm. Then they were hot extruded by a horizontal XCJ300 extruder with a extrusion speed 2 mm/s at 400 °C. The diameter of extruded rods is 15 mm and the extrusion ratio was 16:1.

2.2 Specimen and Experiments

The rods of hot extruded alloy were processed into metallographic specimens with the size of 8mm×8mm×8mm, specimens were taken in the direction perpendicular to the hot

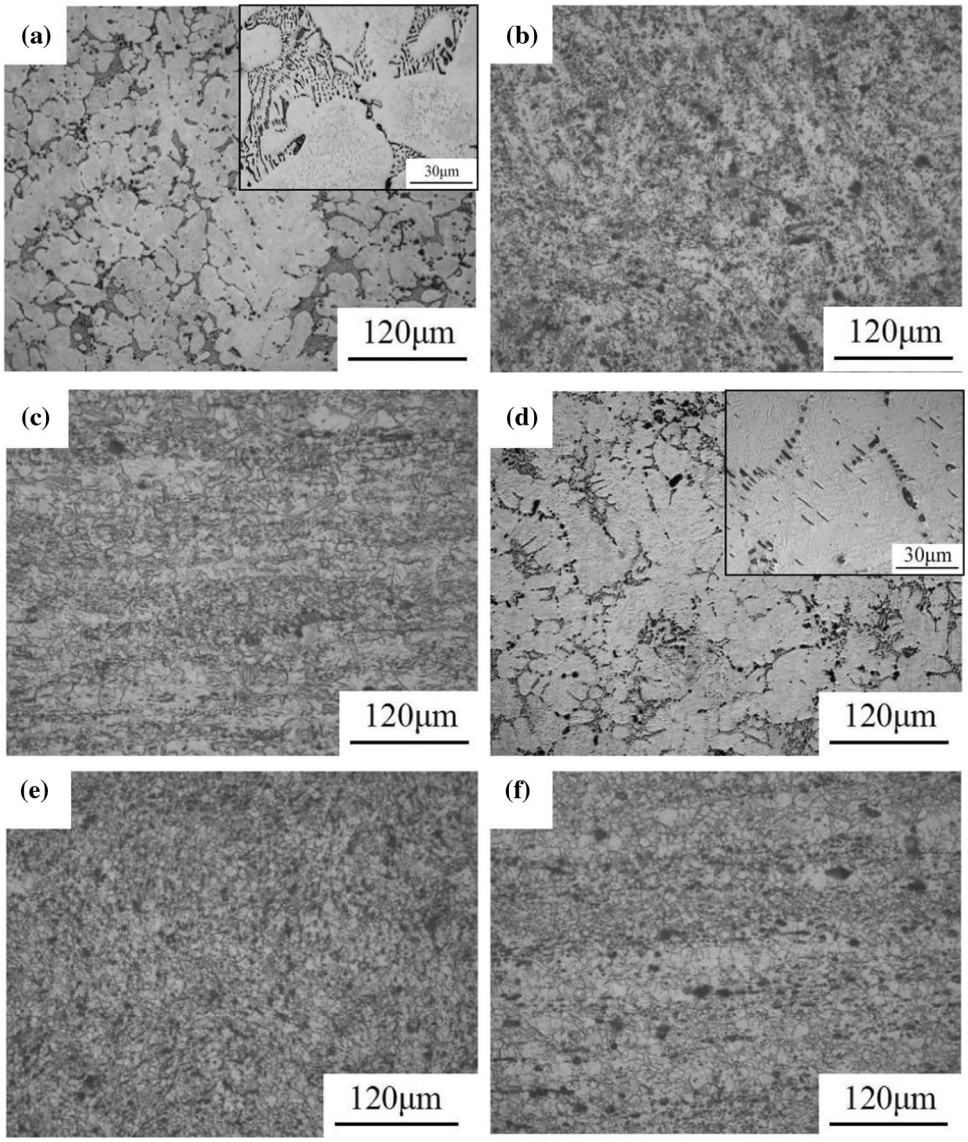

Fig. 2. Optical microstructure of Mg-6Nd-2Al alloy by (a) the as-cast alloy; (b) the as-cast alloy after hot extrusion (TD); (c) the as-cast alloy after hot extrusion (RD); (d) the solid-solution alloy; (e) the solid-solution alloy after hot extrusion (TD); (f) the solid-solution alloy after hot extrusion (RD)

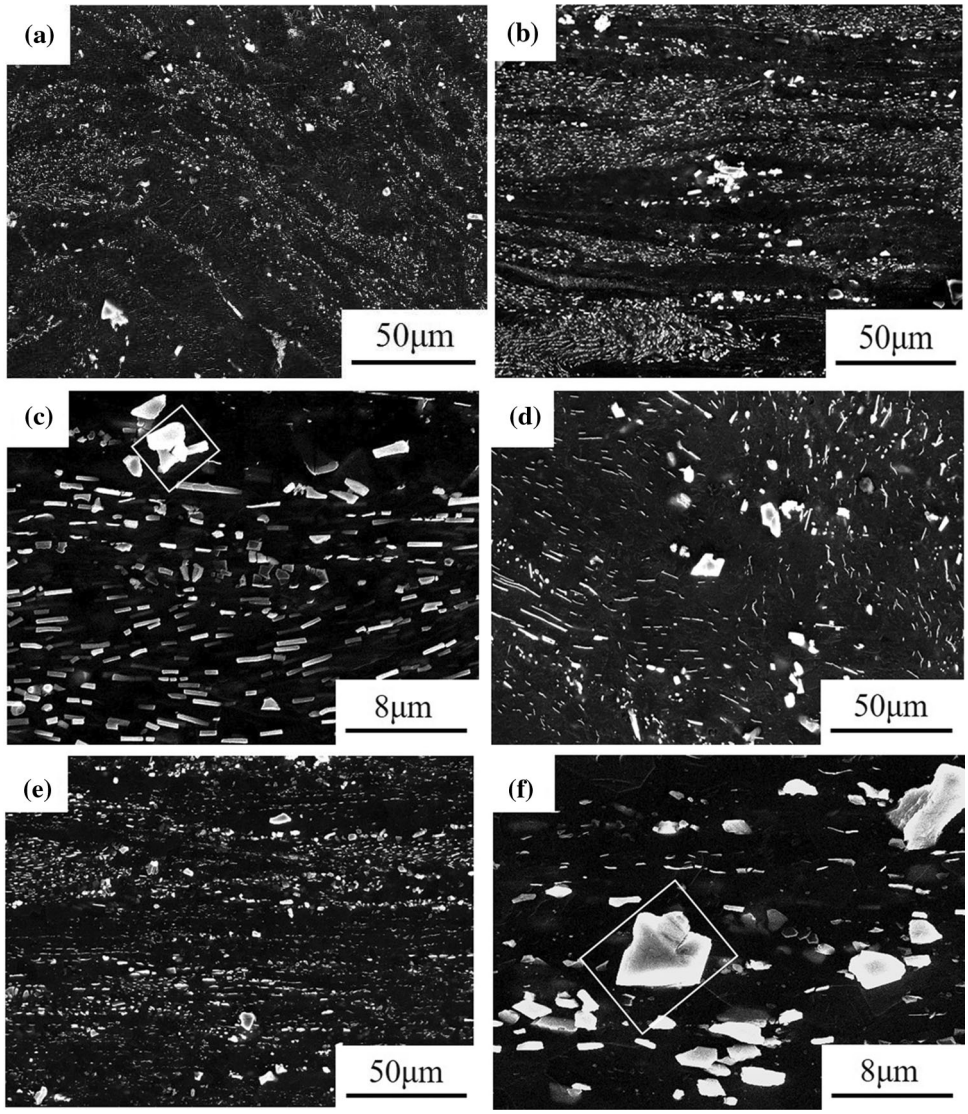

Fig. 3. SEM images of hot extruded Mg-6Nd-2Al alloy by (a) the as-cast alloy after hot extrusion (TD); (b) and (c) the as-cast alloy after hot extrusion (RD); (d) the solid-solution alloy after hot extrusion (TD); (e) and (f) the solid-solution alloy after hot extrusion (RD)

extruded direction (TD) and parallel to the hot extrusion direction (RD), respectively. After pre-grinding and polishing, they were corroded with 2% HNO_3 alcohol solution and Acetic-Picral reagent (10 g picric acid + 15 mL acetic acid + 120 mL ethanol + 20 mL distilled water), afterward the optical microstructure was observed on the optical microscopy (OM-OLYMPUS-BX41 M). X-ray diffractometer (XRD-X´ Pert PRO) was used to analyze the phase of the alloy. The scanning speed is 5°/min, and the scanning angle is from 10° to 80°. The preparation method of XRD specimens is similar to that of the metallographic specimens. The difference is that there is no corrosion after polishing, and it is tested directly after cleaning and drying. The grain orientation, grain size, grain boundary, and texture of the alloys were carried out using the Oxford HKL Channel 5 electron back-scattered diffraction (EBSD) system that assembled on the scanning electron microscope (SEM-APREO-C) with an accelerating voltage of 20 kV and a working distance of 14.4 mm. The specimens were inclined at 70° with a step length of 0.6 μm. Sampling position was parallel to the hot extruded direction. Specimens of EBSD were produced by electrolytic polishing in a solution of 8 mL nitric acid + 12 mL hydrochloric acid + 100 mL alcohol at 20 V for 25 s. The tensile fracture morphology of the alloy was carried out using the SEM. Transmission electron microscope (TEM-JEM-2100) was used to analyze the precipitated phase. Specimens were prepared for TEM using an ion polisher with the ion gun angles of 9°, 6°, and 3°. The room temperature tensile performance test was carried out on the universal tensile testing machine (E44.304-B). The tensile specimen was a rectangular cross-sectional specimen, gage length was 18 mm × 5 mm × 2 mm, and the tensile rate was set to 0.5 mm/min.

3. Results and Discussion

3.1 Microstructure Analysis

In order to identify the phases in the alloys, XRD analysis was carried out and the XRD patterns are shown in Fig.1. It can be seen from the patterns that the diffraction peaks of the as-

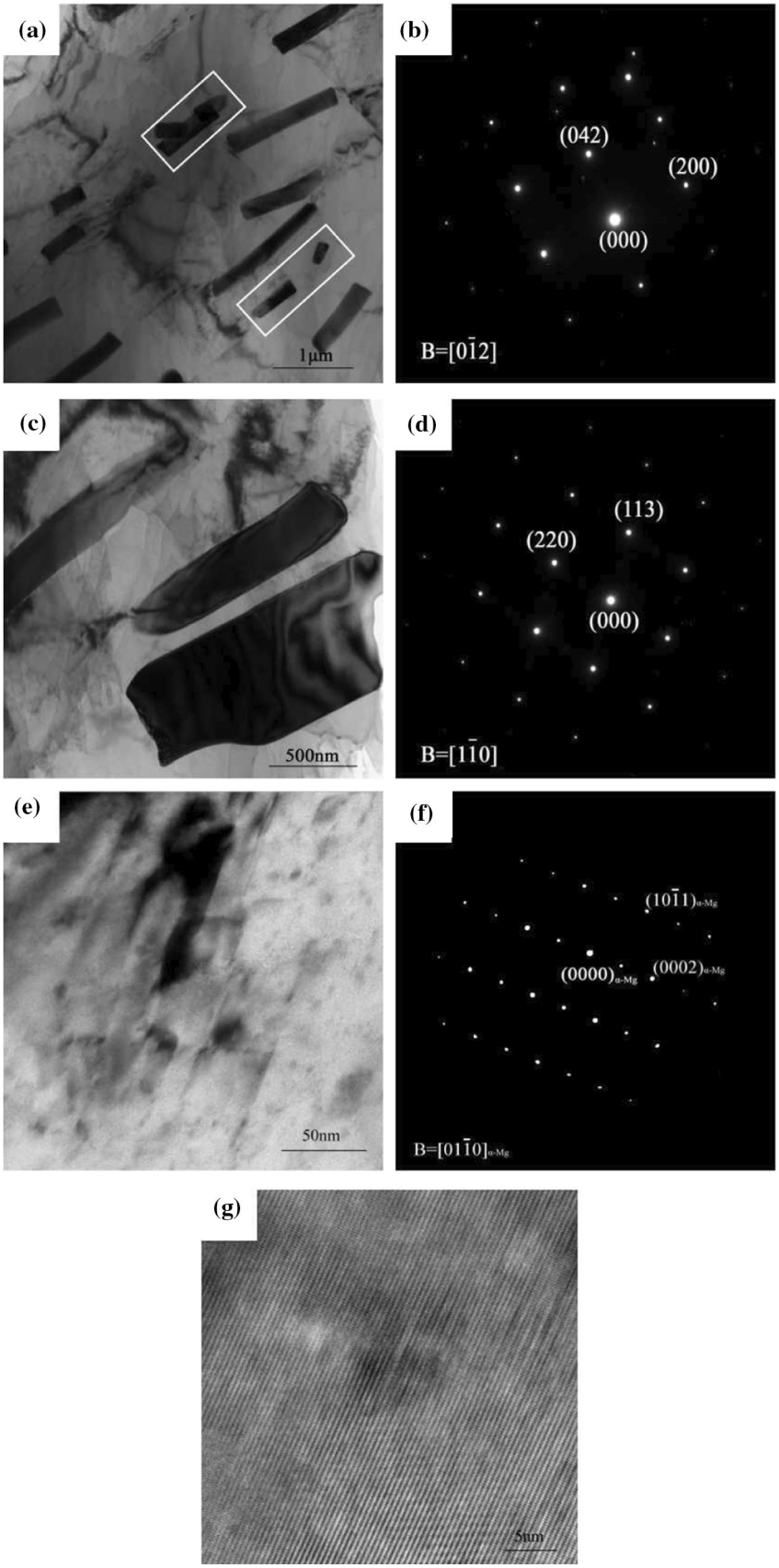
(a)
1μm
(b)
(042)
(200)
(000)
B=[0$\bar{1}$2]
(c)
500nm
(d)
(113)
(220)
(000)
B=[1$\bar{1}$0]
(e)
50nm
(f)
(10$\bar{1}$1)$_{\alpha\text{-Mg}}$
(0000)$_{\alpha\text{-Mg}}$
(0002)$_{\alpha\text{-Mg}}$
B=[01$\bar{1}$0]$_{\alpha\text{-Mg}}$
(g)
5nm

◀**Fig. 4.** TEM images of hot extruded Mg-6Nd-2Al alloy by (a) bright field image of short rod-like precipitation phase of as-cast alloy; (b) corresponding SAED pattern; (c) bright field image of granular-like precipitation phase of as-cast alloy; (d) corresponding SAED pattern; (e) bright field image of needle-like precipitation phase of solid-solution alloy; (f) corresponding SAED pattern; (g) HRTEM image of needle-like precipitation phase

cast alloy after hot extrusion are α-Mg matrix, $Al_{11}Nd_3$ phase, Al_2Nd phase, and $Mg_{12}Nd$ phase. After the solid solution alloy is hot-extruded, compared with the as-cast hot-extruded alloy, the diffraction peaks of the α-Mg matrix and Al_2Nd phase still exist, and the diffraction peak intensity of the Al_2Nd phase is significantly increased, while the diffraction peaks of the $Al_{11}Nd_3$ phase and the $Mg_{12}Nd$ phase disappeared.

Figure 2 shows the microstructure of the Mg-6Nd-2Al alloy with different conditions. The observation direction of the alloy after hot extrusion is TD and RD. The microstructure of as-cast alloy is obvious dendritic crystal morphology, which consists of a large amount of α-Mg matrix, a discontinuous network of strip-shaped $Mg_{12}Nd$ phase and short rod-shaped $Al_{11}Nd_3$ phase at the grain boundary, and a small amount of Al_2Nd phase in the α-Mg matrix (Fig. 2a). During the hot extrusion process, dynamic recrystallization (DRX) is not completely developed. There are still coarse original grains in the deformed microstructure, fine DRX grains are distributed unevenly around them (Fig. 2b). There are a large number of small DRX grains, deformed grains elongated along the extruded direction and broken grains during hot extrusion in the alloy (Fig. 2c). After the as-cast alloy is isothermal treated, most of the second phase distributed at the grain boundary is dissolved in the matrix, and the amount is significantly reduced, but the granular Al_2Nd phase can still be observed, the needle-like Al_2Nd phase is precipitated in the α-Mg matrix (Fig. 2d). For the solid-solution alloy after hot extrusion, the deformed microstructure is relatively uniform, but there are still a small number of smaller DRX grains in the alloy (Fig. 2e). The DRX grains split the coarse original grains of the alloy, and the original microstructure is greatly reduced and the DRX microstructure is obviously increased (Fig. 2f). In addition, comparing the as-cast alloy with solid-solution alloy, it is obvious that the microstructure of the solid-solution alloy is more uniform. The grains of the hot extruded alloy are obviously finer than those of the alloy without hot extrusion, also the microstructure distribution is more uniform. When the observation is parallel to the extruded direction, both the as-cast and solid-solution alloys have directionality and are linearly distributed along the hot extruded direction.

Figure 3 shows the SEM photograph of the Mg-6Nd-2Al alloy after hot extrusion. The observations were along TD and RD. The second phases are not uniformly distributed after the as-cast alloy is hot extruded. And the DRX occurs in the second phase enriched area. Among them, some of the second phases are more obviously broken, and some are not completely broken. For example, the short rod-shaped $Al_{11}Nd_3$ phase and the strip-shaped $Mg_{12}Nd$ phase are both broken into fine particles, while the granular Al_2Nd phase is partially broken (Fig. 3a). The microstructure of as-cast alloy after hot extrusion was observed from RD. The short rod-shaped $Al_{11}Nd_3$ phase and the irregular strip-shaped $Mg_{12}Nd$ phase between the dendrites of the α-Mg matrix are distributed along the extruded direction. Plastic rheology occurs and obvious parallel strips are formed. The α-Mg matrix strips and the second phase strips were stacked in sequence (Fig. 3b). In the solid-solution alloy after hot extrusion observed from TD, the second phase is more evenly distributed. The needle-shaped Al_2Nd phase is flattened or deformed, and more significant torsion occurs. At the same time, part of the granular Al_2Nd phase is not completely broken (Fig. 3d). In the solid-solution alloy after hot extrusion, the direction of the needle-like Al_2Nd phase in the alloy becomes uniform and the distribution becomes more even. Some phases are broken, while some are not and they both are distributed along the extruded direction (Fig. 3e). Parts of the second phase are solid dissolved into the matrix after isothermal treatment, so the overall phase content is reduced and the distribution is more uniform. Compared with the as-cast alloy after hot extrusion, the number of granular Al_2Nd phases in the solid-solution alloy after hot extrusion is significantly reduced, but the number of needle-shaped Al_2Nd phases is increased. The granular Al_2Nd phase could provide nucleation place to refine grains, so that the grain size of the solid solution alloy after hot extrusion is larger than that of the as-cast alloy after hot extrusion (Ref 18). In addition, cracks could be observed on some broken second phases, and the direction of the cracks is perpendicular to the hot extruded direction, as shown in Fig. 3(c) and (f). During the hot extrusion process, the alloy is subjected to tensile stress along the hot extrusion direction and compressive stress perpendicular to the extrusion direction. Therefore, when the tensile stress along the hot extrusion direction is large enough, it would result in cracks perpendicular to the hot extrusion direction on the second phase.

In order to further analyze the microstructure of the hot extruded Mg-6Nd-2Al alloy, TEM was used to observe the alloy along RD. Figure 4 shows a TEM photograph of the second phases in hot extruded Mg-6Nd-2Al alloy. From the bright field image of the short rod-shaped $Al_{11}Nd_3$ phase in the as-cast alloy after hot extrusion, it can be seen that the $Al_{11}Nd_3$ phase is crushed and fractured (Fig. 4a). The $Al_{11}Nd_3$ phase has an orthorhombic microstructure, and its lattice constant is a = 0.4359 nm, b = 1.2924 nm, c = 1.0017 nm (Ref 19). The incident electron beam is used to calibrate the corresponding selected area electron diffraction (SAED) pattern along the $[0\bar{1}2]$ direction (Fig. 4b). From the bright field image of the granular Al_2Nd phase in as-cast alloy after hot extrusion, it can be observed that the entire granular Al_2Nd phase is squeezed and broken into two parts (Fig. 4c). The Al_2Nd phase has a face-centered cubic structure, and its lattice constant is a = 0.8000nm (Ref 19). The incident electron beam is used to calibrate the corresponding SAED pattern along the $[1\bar{1}0]$ direction (Fig. 4d). In the solid-solution alloy after hot extrusion, there are fine needle-like Al_2Nd phases precipitated along the basal plane {0002}α-Mg, the density of the precipitated phase is relatively low, the length is about 60-80nm, and the thickness is smaller than 1nm (Fig. 4e). And the incident electron beam is used to calibrate the solid-solution alloy after hot extrusion along the $[11\bar{2}0]_{\alpha\text{-Mg}}$ direction. Observing the corresponding SAED pattern at the same time, it can be found that no additional diffraction spots exist (Fig. 4f). In the high-resolution transmission electron microscope (HRTEM) photograph of the needle-like Al_2Nd phases, some needle-like second phases with shorter size and thinner thickness can be observed, and the second phases are in a coherent relationship with the matrix (Fig. 4g).

In order to further analyze the effect of the initial microstructure on the hot extruded Mg-6Nd-2Al alloy, the as-cast and solid-solution alloys after hot extrusion are characterized by EBSD. Figure 5 shows the IPF maps and grain size distribution of the as-cast and solid-solution alloys along RD. The grain size of the solid-solution alloy after hot extrusion is relatively larger than that of the as-cast alloy after hot extrusion (Fig. 5a and c). The grain size of the as-cast alloy after hot extrusion varies from 0.68μm to 17.96μm, and the average grain size is 2.98 μm (Fig. 5b). The grain size of the solid-solution alloy after hot extrusion varies from 0.68μm to 12.92 μm, and the average grain size is 3.68μm (Fig. 5d). The average grain size of the hot extruded alloy after isothermal treatment has increased. After hot extrusion, the grains are flattened and elongated differently along the hot extruded direction, and no twins are found. In addition, DRX occurs in

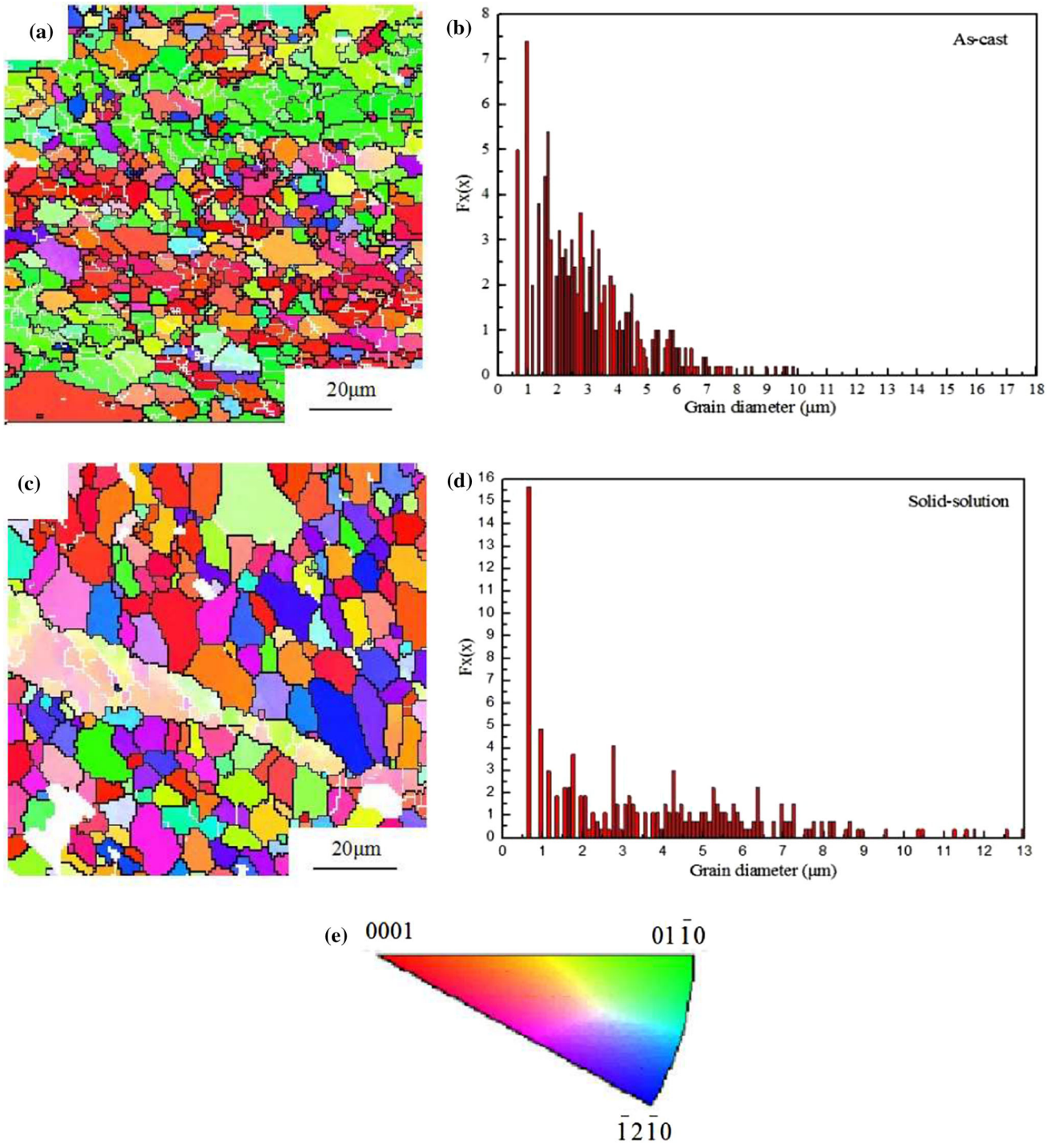

Fig. 5. EBSD maps and grain size distribution of hot extruded Mg-6Nd-2Al alloy by (a) the as-cast alloy after hot extrusion; (b) corresponding grain size distribution; (c) the solid-solution alloy after hot extrusion; (d) corresponding grain size distribution; (e) inverse pole figure

both alloys. That is because a large amount of the second phase is crushed to form smaller ones during the extruded process. According to the particle-stimulated nucleation (PSN) theory (Ref 20), these the second phase of micron-sized particles can promote the nucleation and progress of DRX. The solid-solution alloy after hot extrusion contains more needle-like phases. Compared with it, the content of granular second phase in the as-cast alloy after hot extrusion is more, which promotes the nucleation of DRX and produces smaller size DRX grains. The DRX are not developed completely in both alloys because the rare earth element Nd has an inhibitory effect on DRX.

Figure 6 shows the DRX distribution of as-cast and solid-solution alloys after hot extrusion along RD. The blue grains are DRX grains, the yellow grains are substructure grains, and the red grains are deformed grains. It can be found that DRX grains appear at the grain boundaries, and the DRX grains in the solid-solution alloy after hot extrusion have grown larger than the as-cast alloy after hot extrusion. The DRX grains, substructure grains, and deformed grains in the as-cast alloy after hot extrusion account for 15.7%, 47.8%, and 36.5%, while these three grains in the solid-solution alloy after hot extrusion account for 33.1%, 54.9%, and 11.9%. In the two alloys, the proportion of substructure grains is close, the proportion of deformed grains in the as-cast alloy after hot extrusion is larger, and the proportion of DRX grains in the solid-solution alloy after hot extrusion is larger (Fig. 6b and d).

Figure 7 shows the grain boundary distribution map and misorientation distribution map of hot extruded Mg-6Nd-2Al alloy, in which the green thin line represents the small-angle grain boundary (2°-15°), and the red thin line represents the large-angle grain boundary ($>15°$). The number of small-angle grain boundaries in as-cast alloys after hot extrusion is significantly greater than that in solid-solution alloys after hot extrusion, while large-angle grain boundaries are significantly less than those in solid-solution alloys after hot extrusion (Fig. 7a and c). The reason is that the sub-grain boundaries continuously absorb dislocation during the thermal deformation process, and the angles continue to increase, which leads to the transformation of small-angle grain boundaries into large-angle grain boundaries. In other words, the sub-grain transforms into

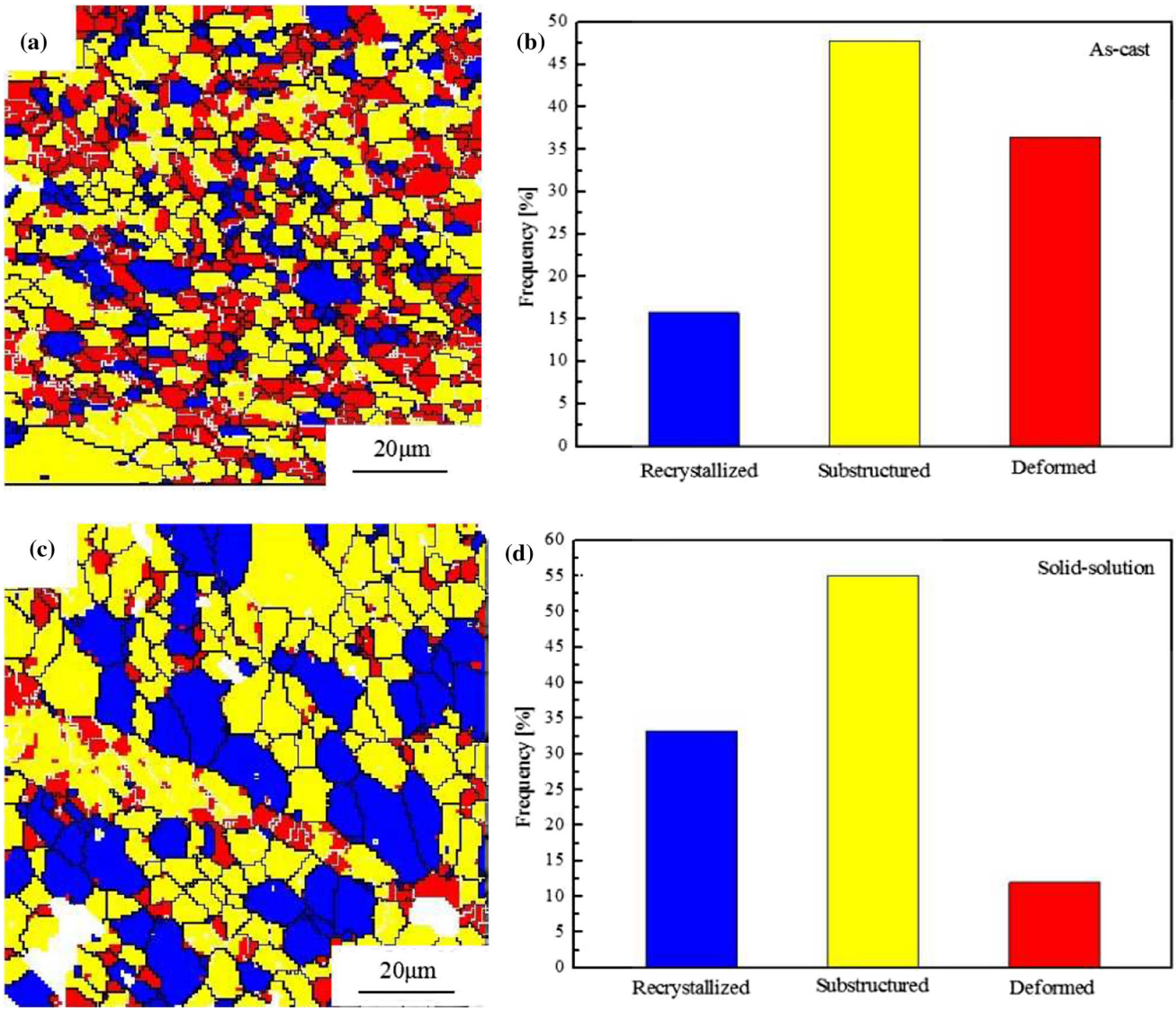

Fig. 6. DRX map and histogram of hot extruded Mg-6Nd-2Al alloy by (a) DRX map of as-cast alloy after hot extrusion; (b) corresponding DRX histogram; (c) DRX map of solid-solution alloy after hot extrusion; (d) corresponding DRX histogram

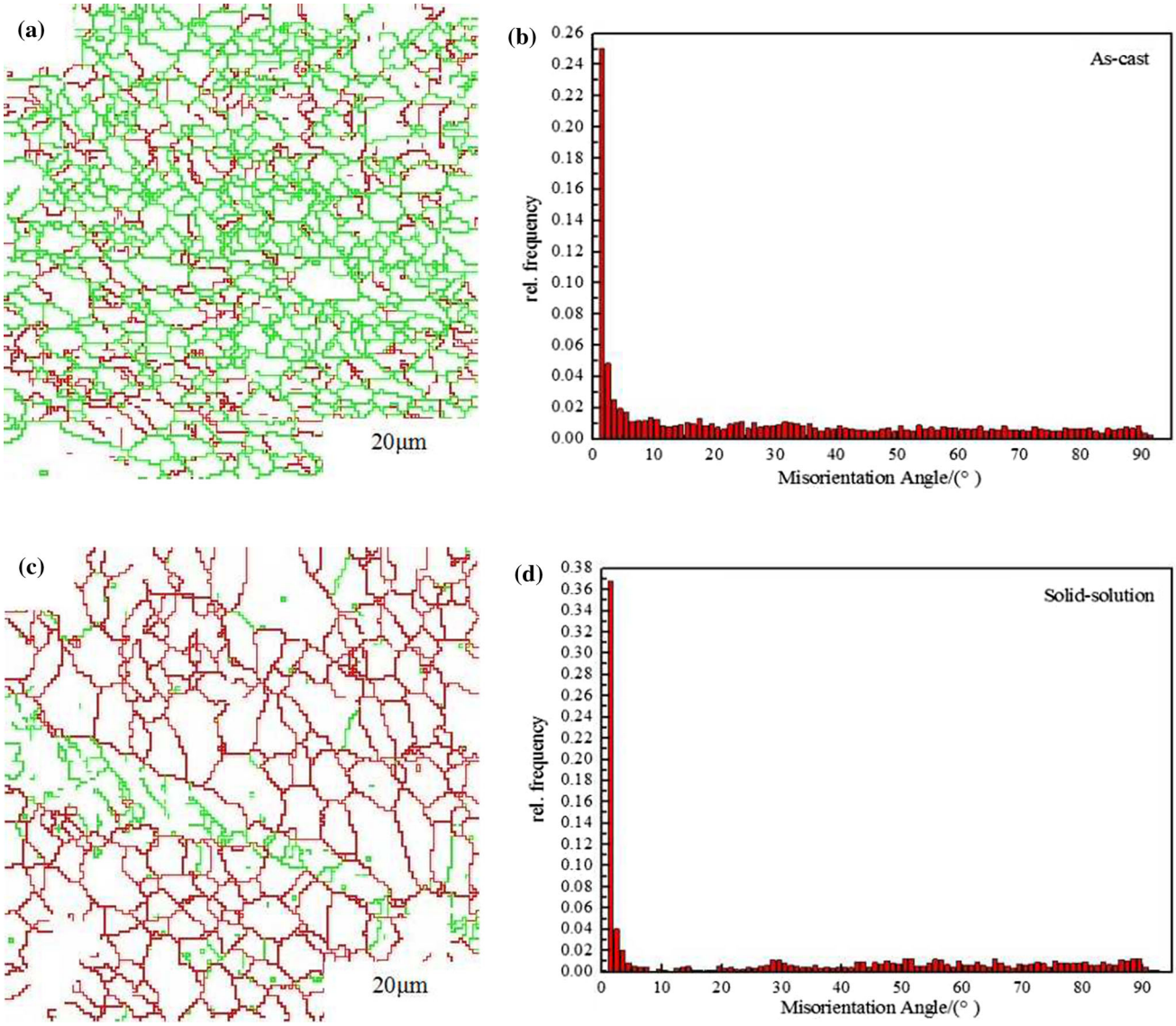

Fig. 7. Grain boundaries maps and misorientation angle distribution of hot extruded Mg-6Nd-2Al alloy by (a) grain boundaries map of as-cast extruded alloy; (b) corresponding misorientation angle distribution; (c) grain boundaries maps of solid-solution extruded alloy; (d) corresponding misorientation angle distribution

real grains (Ref 21, 22). The misorientation of the two alloys shows a peak at 1.5°, and then gradually decreased, which is caused by the migration of grain boundaries (Fig. 7b and d). The small-angle grain boundary with a misorientation less than 15° in the solid-solution alloy after hot extrusion is less than that of the as-cast alloy after hot extrusion. After the as-cast alloy undergoes isothermal treatment, more dislocation movement makes the small-angle grain boundaries absorb dislocations and transform into DRX grains, and the degree of DRX is improved obviously.

In order to analyze the texture change in the hot extruded Mg-6Nd-2Al alloy, it is necessary to analyze the pole figures of the alloy, as shown in Fig. 8. A typical extruded fiber texture appears in the as-cast alloy after hot extrusion, which is (0001) texture perpendicular to the hot extruded direction (Fig. 8a). The maximum pole density of the as-cast alloy after hot extrusion is 14.74, larger than the maximum pole density of the solid-solution alloy after hot extrusion, which is 12.61 (Fig. 8a). Besides, the texture distribution of the as-cast alloy after hot extrusion is relatively uniform, while the texture of solid-solution alloy after hot extrusion distributes unevenly. The maximum pole density of the isothermal treatment alloy after hot extrusion is decreased, and the texture-weakening phenomenon appears. The main reasons are as follows. First of all, the content of DRX grains in the solid-solution alloy after hot extrusion is larger, and the base texture strength of the DRX grains is weak. The DRX area is smaller in the as-cast alloy after hot extrusion, the basal texture strength is stronger (Ref 16), which could play a role in texture strengthening. Secondly, the average grain size of the as-cast alloy after hot extrusion is small, which leads to an increase in grain boundaries per unit volume, hinders the movement of dislocations, and produces a strong fine-grain strengthening effect. The fine grains make the rotation of the grains and the movement of the grain boundaries much easier, which in turn cause the changes in grain orientation (Ref 23). Furthermore, it can be found that not only (0001) basal surface slipped, but also non-basal surface slipped in the as-cast alloy after hot extrusion (Fig. 8a). In other

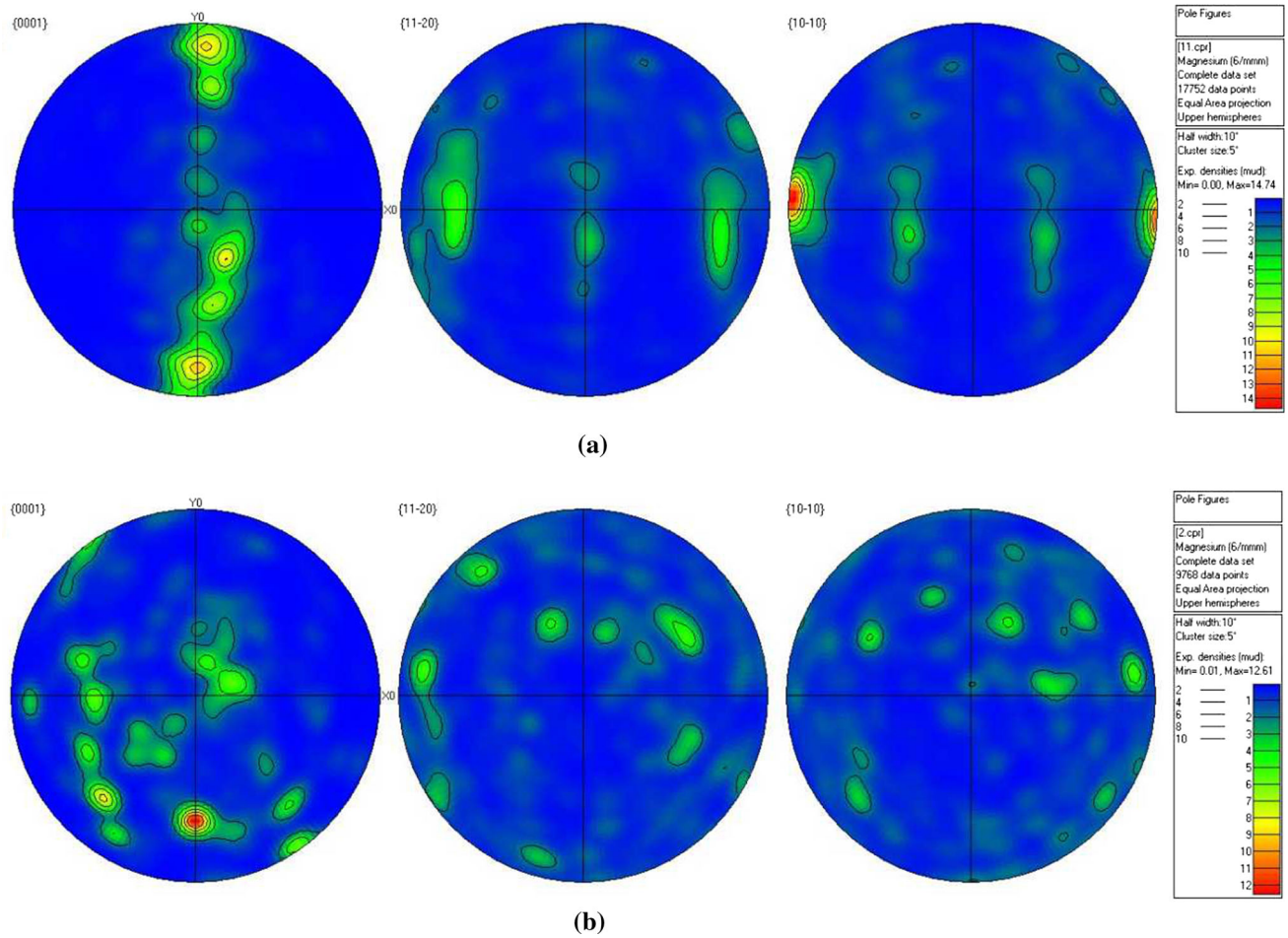

Fig. 8. Pole figures referring to the RD for hot extruded Mg-6Nd-2Al alloy by (a) the as-cast alloy after hot extrusion; (b) the solid-solution alloy after hot extrusion

words, there is a strong {01-10} prismatic surface texture, which is approximately symmetrically distributed to the two poles along the hot extruded direction. The {01-10} prism surface dose not form an obvious preferred orientation in the solid-solution alloy after hot extrusion.

4. Mechanical Properties Analysis

The room temperature tensile properties of the as-cast and solid-solution Mg-6Nd-2Al alloys after hot extrusion are shown in Fig. 9. The distribution, morphology, and quantity of the second phase of alloys are different after hot extrusion, resulting in different mechanical properties. The tensile strength and yield strength of the as-cast and solid-solution alloys after hot extrusion are 271.2MPa, 229.5MPa, 247.8MPa, and 176.1MPa, respectively. The tensile strength and yield strength of the as-cast alloy after hot extrusion are both higher than those of the solid-solution alloy after hot extrusion. The main reasons are as follows. First of all, the average grain size of the as-cast alloy after hot extrusion is small, which can produce strong fine-grain strengthening effect. At the same time, there are more grain boundaries per unit volume, which hinder the movement of dislocations. The second phase is broken during the hot extruded process, forms fine and dispersed second-

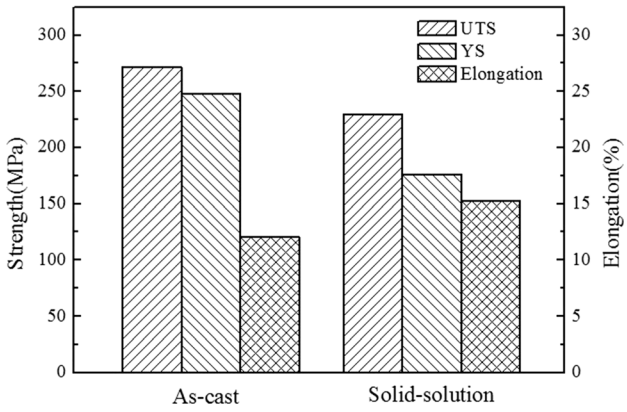

Fig.9. Mechanical properties of hot extruded Mg-6Nd-2Al alloy at room temperature

phase particles, which would also play a role in hindering the movement of dislocations. Thus, the ability of the alloy to resist plastic deformation and the strength of the alloy are improved (Ref 24). Secondly, there are more second phases in the as-cast alloy after hot extrusion, especially the content of the granular Al2Nd phase, which plays a role in second phase strengthening and dispersion strengthening. Finally, there are strong base and non-base textures in the alloy, which have a texture strengthen

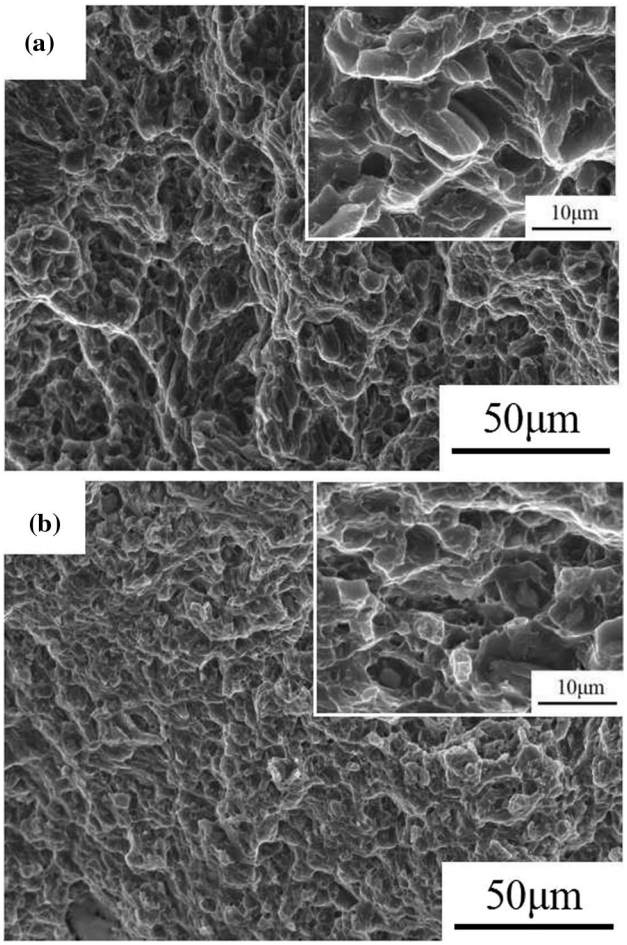

Fig. 10. Tensile fracture morphology of Mg-6Nd-2Al alloy for (a) the as-cast alloy after hot extrusion; (b) the solid-solution alloy after hot extrusion

effect on the alloy. Compared the as-cast alloy with the solid-solution alloy after hot extrusion, the elongation of the former is 78.9% of the latter. This is because the grain size of the as-cast alloy after hot extrusion distributes inconsistently, which results in the different ability of each grain to resist plastic deformation. Consequently, the elongation of as-cast alloy after hot extrusion is lower. Moreover, the needle-like Al_2Nd phase in the solid-solution alloy after hot extrusion can effectively improve the ductility of the alloy.

Figure 10 shows the tensile fracture morphology of the as-cast and solid-solution Mg-6Nd-2Al alloy after hot extrusion. It can be observed from the figures that there are a large number of dimples in the fracture surface of the alloy. After hot extrusion, the fracture mode of the alloy transforms to ductile fracture. Figure 10a shows the tensile fracture morphology of the as-cast alloy after hot extrusion with deep dimples. In contrast, observing the tensile fracture morphology of the solid solution alloy after hot extrusion, the dimples are not obvious and shallow, and the strength is lower than that of the as-cast alloy after hot extrusion (Fig. 10b). The main reason is that after solid-solution treatment, a large amount of Al_2Nd phase precipitated in the matrix. After hot extrusion, this phase was broken and caused the second phase particles to be tightly distributed. At the same time, cracks are easy to expand, which inhibit the increase in strength.

5. Conclusions

Based on the experimental results and discussions in the present work, the conclusions can be drawn as follows:

1. The as-cast alloy after hot extrusion is composed of α-Mg matrix, short rod-shaped $Al_{11}Nd_3$ phase, strip-shaped $Mg_{12}Nd$ phase, and granular Al_2Nd phase. Parts of the phases are crushed after hot extrusion. The granular Al_2Nd phase can still be observed in the solid-solution alloy after hot extrusion, and the needle-shaped Al_2Nd phase is precipitated in the α-Mg matrix, which is flattened or deformed. The average grain size of as-cast is smaller than that of solid-solution alloys after hot extrusion. The average grain sizes are 2.98μm and 3.68μm, respectively. DRX occurs in the alloys and no twins are found.
2. A typical extruded fiber texture appears in the as-cast alloy after hot extrusion, that is (0001) perpendicular to the extruded direction. The maximum pole density of the as-cast alloy after hot extrusion is 14.74, and the texture distribution is relatively uniform. The maximum pole density of the solid-solution alloy after hot extrusion is relatively smaller, which is 12.61. Moreover, the texture distribution is uneven. There is also non-basal surface slipping in the as-cast alloy after hot extrusion, and the {01-10} prismatic surface texture is strong. In the solid-solution alloy after hot extrusion, no obvious preferred orientation is formed.
3. The tensile strength and yield strength of as-cast and solid-solution alloys after hot extrusion are 271.2MPa, 229.5MPa, 247.8MPa, and 176.1MPa, respectively. The tensile strength and yield strength of the as-cast alloy after hot extrusion are higher than those of the solid-solution alloy after hot extrusion. The elongation of the as-cast alloy after hot extrusion is 12.1%, lower than that of the solid-solution alloy after hot extrusion, which is 15.3%.
4. By studying the effect of initial microstructure conditions on the microstructure and mechanical properties of the hot extruded Mg-6Nd-2Al alloy. It can be concluded that for the as-cast Mg-6Nd-2Al alloy after hot extrusion, there are more content and types of the second phase, and the alloy has high strength. The content of the second phase in the solid-solution alloy after hot extrusion is low, and the granular Al_2RE phase is conducive to the plasticity of the alloy.

Acknowledgments

The authors gratefully acknowledge the financial support from the Heilongjiang Province Natural Science Foundation (No. E2018045).

References

1. J. He, B. Jiang, Q. Yang, X. Li, X. Xia and F. Pan, Influence of Pre-hardening on Microstructure Evolution and Mechanical Behavior of AZ31 Magnesium Alloy Sheet, *J. Alloys Compd.*, 2015, **621**, p 301–306.

2. E. Aghion, B. Bronfin and D. Eliezer, The Role of the Magnesium Industry in Protecting the Environment, *J. Mater. Process. Tech.*, 2001, **117**(3), p 381–385.
3. L. Wang, E.J. Guo, W.Y. Jiang, Y.C. Feng, S.C. Zhao, Y.K. Fu and H.T. Chen, Effect of Al Addition on Microstructure and Mechanical Properties of As-cast Mg-4Y-3Nd Alloy, *Philos. Mag.*, 2020, **100**(2), p 234–247.
4. J.H. Zhang, Z. Leng, S.J. Liu, M.L. Zhang, J. Meng and R.Z. Wu, Structure stability and mechanical properties of Mg-Al-based alloy modified with Y-rich and Ce-rich misch metals, *J. Alloys Compd.*, 2011, **509**(20), p 187–193.
5. K. Hantzsche, J. Bohlen, J. Wendt, K.U. Kainer, S.B. Yi and D. Letzig, Effect of Rare Earth Additions on Microstructure and Texture Development of Magnesium Alloy Sheets, *Scr. Mater.*, 2021, **63**, p 725–730.
6. Q. Zhang, Q.A. Li, X.T. Jing and X.Y. Zhang, Microstructure and Mechanical Properties of Mg-10Y-2.5Sm Alloy, *J. Rare. Earths.*, 2010, **28**, p 375–377.
7. J.C. Dai, M.A. Easton, S.M. Zhu, G.H. Wu and W.J. Ding, Grain Refinement of Mg-10Gd Alloy by A1 Additions, *J. Mater. Res.*, 2012, **27**(21), p 2790–2797.
8. L. Wang, Y.C. Feng, L.P. Wang, Y.H. Chen and E.R. Guo, Effect of Al on Grain Refinement and Mechanical Properties of Mg-3Nd Casting Alloy, *J. Mater. Eng. Perform.*, 2018, **27**(5), p 2099–2109.
9. C.L. Wang, J.C. Dai, W.C. Liu, L. Zhang and G.H. Wu, Effect of A1 Additions on Grain Refinement and Mechanical Properties of Mg-Sm Alloys, *J. Alloys Compd.*, 2015, **620**, p 172–179.
10. D. Liu, J.F. Song, B. Jiang, Y. Zeng, Q.H. Wang, Z.T. Jiang, B. Liu, G.S. Huang and F.S. Pan, Effect of Al Content on Microstructure and Mechanical Properties of As-cast Mg-5Nd Alloys, *J. Alloys Compd.*, 2018, **737**, p 263–270.
11. J.L. Wang, Y.C. Guo, J.P. Li, Z. Yang and S. Kamado, Microstructure, Texture and Mechanical Properties of Extruded Mg-5Al-2Nd-0.2Mn Alloy, *J. Alloys Compd.*, 2015, **635**, p 100–107.
12. M.O. Pekguleryuz and A.A. Kaya, Creep Resistant Magnesium Alloys for Powertrain Applications, *Adv. Eng. Mater.*, 2003, **5**(12), p 866–878.
13. M. Shahzad and L. Wagner, Influence of Extrusion Parameters on Microstructure and Texture Developments, and Their Effects on Mechanical Properties of the Magnesium Alloy AZ80, *Mater. Sci. Eng. A*, 2008, **506**(1), p 141–147.
14. T. Murai, S. Matsuoka, S. Miyamoto and Y. Oki, Effects of Extrusion Conditions on Microstructure and Mechanical Properties of AZ31B Magnesium Alloy Extrusions, *J. Mater. Process. Tech.*, 2003, **141**(2), p 207–212.
15. B. Pourbahari, H. Mirzadeh and M. Emamy, Toward Unraveling the Effects of Intermetallic Compounds on the Microstructure and Mechanical Properties of Mg-Gd-Al-Zn Magnesium Alloys in the As-Cast, Homogenized, and Extruded Conditions, *Mater. Sci. Eng. A*, 2017, **680**, p 39–46.
16. N.L. Li, G.J. Huang, R.L. Xin and Q. Liu, Effect of Initial Texture on Dynamic Recrystallization and Deformation Mechanisms in AZ31 Mg Alloy Extruded at 573 K, *Mater. Sci. Eng. A*, 2013, **569**, p 18–26.
17. Y.C. Feng, F.S. Zhang, Y.L. Chen, S.C. Zhao, L.P. Wang and E.J. Guo, Effect of Initial Microstructure on Microstructure and Mechanical Properties of Hot-extruded Mg-6Al-2Ca-2Sm Alloy, *Rare. Metal. Mat. Eng.*, 2020, **49**(12), p 4246–4252. (**(in Chinese)**)
18. J.H. Zhang, J. Wang, X. Qiu, D.P. Zhang, T. Zheng, X.D. Niu, D.X. Tang and J. Meng, Effect of Nd on the Microstructure, Mechanical Properties and Corrosion Behavior of Die-Cast Mg-4Al-based Alloy, *J. Alloys Compd.*, 2008, **464**(1), p 556–564.
19. S.H. Kim, D.H. Kim and N.J. Kim, Structure and Properties of Rapidly Solidified Mg-Al-Zn-Nd Alloys, *Mater. Sci. Eng. A*, 1997, **226**, p 1030–1034.
20. J.D. Robson, D.T. Henry and B. Davis, Particle Effects on Recrystallization in Magnesium-Manganese Alloys: Particle-Stimulated Nucleation, *Acta Mater.*, 2009, **57**(9), p 2739–2747.
21. A.S.H. Kabir, M. Sanjari, J. Su, I.H. Jung and S. Yue, Effect of Strain-Induced Precipitation on Dynamic Recrystallization in Mg-Al-Sn Alloys, *Mater. Sci. Eng. A*, 2014, **616**(20), p 252–259.
22. K. Huang and R.E. Logé, A Review of Dynamic Recrystallization Phenomena in Metallic Materials, *Mater Des.*, 2016, **111**(5), p 548–574.
23. Z.H. Chen, *Deformed Magnesium Alloy*, Chemical Industry Press, Beijing , 2005, p 81. (**(in Chinese)**)
24. C. Xu, M.Y. Zheng, S.W. Xu, K. Wu, E.D. Wang, S. Kamado, G.J. Wang and X.Y. Lv, Ultra High-Strength Mg–Gd–Y–Zn–Zr Alloy Sheets Processed by Large-Strain Hot Rolling and Ageing, *Mater. Sci. Eng. A*, 2012, **547**, p 93–98.